Chemical Geology 501 (2018) 1–11

Contents lists available at ScienceDirect

Chemical Geology

journal homepage: www.elsevier.com/locate/chemgeo

Controls on lithium concentration and diffusion in zircon

J.T. Sliwinski*, N. Kueter, F. Marxer, P. Ulmer, M. Guillong, O. Bachmann

ETH Zürich, Institute for Geochemistry & Petrology, Zürich, Switzerland

ARTICLE INFO

Editor: D.B. Dingwell

Keywords:
Lithium
Zircon
Diffusion speedometry
Magma chamber processes
Melt inclusions
Piston cylinder

ABSTRACT

Thermal annealing of zircons prior to uranium-lead dating by laser ablation inductively coupled plasma mass spectrometry is a commonly-implemented procedure which improves data accuracy and precision by partially repairing radiation damage from the decay of uranium and thorium. However, it also leads to significantly higher concentrations of lithium in the zircon lattice, which become positively correlated with trivalent yttrium and rare earth elements. Prior to such treatments, zircons typically contain lithium below detection limits (typically $< 0.55\,\mu g\,g^{-1}$), unless correlated with lanthanum and aluminum (i.e., melt/mineral inclusion tracer elements). This suggests that lithium in zircon is primarily sequestered within inclusions, and is able to permeate the crystal lattice to couple with yttrium and rare earth elements during the thermal annealing procedure. This process occurs 2–3 orders of magnitude faster than diffusion experiments have previously determined, indicating that another diffusion mechanism may apply. A model is proposed, whereby: (i) charge compensation of stoichiometrically over-abundant trivalent cations under water-rich magmatic conditions is likely accomplished by hydrogen, given the incompatibility of lithium in zircon and the abundance of hydrogen. However, (ii) conditions that are high temperature and low pressure (characteristic of both thermal annealing and the syn-eruptive environment), drive silicate melt inclusions to exsolve water, generating a motive force for both hydrogen and lithium from inclusions to permeate the lattice in order to reestablish electrochemical equilibrium between the interior and exterior of the zircon. To test the pressure dependency of lithium migration in the zircon lattice, thermal annealing experiments were performed at 850 °C and 1 bar, 2 kbar and 6 kbar using zircons from the Fish Canyon Tuff. The experiments demonstrate that thermal annealing at 2 and 6 kbar inhibits lithium mobility, with zircons registering lithium concentrations below detection limits similar to controls. The experimental results suggest that lithium concentrations in zircon are vulnerable to rapid perturbation by decompression (concurrent with high temperatures), which further indicate that lithium-in-zircon diffusion data should be interpreted with caution.

1. Introduction

The lithophilic character of lithium, combined with its high mobility in geological materials, make it a prime target for studying timescales of geological processes. Its low atomic weight makes it a rapid diffuser, while the large mass difference between its two stable isotopes allow for significant mass-dependent fractionation under both low- and high-temperature conditions. A variety of geological processes can be traced by Li diffusion and isotopic fractionation, including weathering and fluid-rock interactions (Rudnick et al., 2004), early solar system formation (Magna et al., 2006) and timescales of magmatic processes through mineral diffusion studies (Giletti and Shanahan, 1997; Coogan et al., 2005; Dohmen et al., 2010; Rubin et al., 2017). Studies of Li in zircon are particularly attractive due to the resilience of the zircon lattice and the potential for simultaneous diffusional, geochronological (i.e., U-Th-Pb) and geothermometric studies (i.e., Ti-in-zircon; see Ferry and Watson, 2007). This has spurred recent interest in developing reference materials (Li et al., 2011; Gao et al., 2015) as well as characterization of well-known zircon suites and interpretations of metamorphic and magmatic storage conditions (Ushikubo et al., 2008; Bouvier et al., 2012; Trail et al., 2016; Rubin et al., 2017). More recent analytical advances have allowed the detection of Li at spatial resolutions $< 1\,\mu m$ and concentrations $\sim 1\,ng\,g^{-1}$ by nanoscale secondary ion mass spectrometry (NanoSIMS), potentially allowing for resolution of sub-millennial diffusional timescales (Rubin et al., 2017). However, given the mobility of Li in minerals to syn- and post-depositional processes in volcanic units (Ellis et al., 2015; Ellis et al., 2018), it is important to examine external factors that may affect Li diffusion profiles in zircon. For this, it is necessary to first take note of the mechanisms of Li substitution in zircon.

* Corresponding author.
E-mail address: Jakub.sliwinski@erdw.ethz.ch (J.T. Sliwinski).

https://doi.org/10.1016/j.chemgeo.2018.09.038
Received 15 June 2018; Received in revised form 28 August 2018; Accepted 29 September 2018
Available online 02 October 2018

Table 1
Sample details and treatment.

Unit	Region[a]	Description	Treatment[b]			No. samples	Code
			None	Δ	CA		
Mesa Falls Tuff	YS	Rhyolitic ignimbrite	x	x		1	N/A
Fish Canyon Tuff	SJ	Dacitic ignimbrite	x	x		2	N/A
Cebolla Creek Tuff	SJ	Dacitic ignimbrite	x		x	1	SRM07
Stewart Peak	SJ	Intrusive dacite	x		x	1	SRM09
Fisher Dacite lava	SJ	Dacitic lava	x		x	1	SRM19
pre-CRT Dacite	SJ	Dacitic breccia	x		x	1	SRM21
Nelson Mountain Tuff	SJ	Dacitic-rhyolitic ignimbrite	x	x		9	**17SJ**02, 03, 04, 09, 16, 17, 18, 19
Plutonic							
Mount Princeton	SJ	Quartz monzonite	x	x		10	Untreated: **171516**-3, 4.5, 6, 9, C; Annealed: **17SJ**11, 12, 13, 14, 15
Mount Princeton dykes	SJ	Intrusive dacites		x		5	**71416**_A, B2, C, E, F
Experimental							
Fish Canyon Tuff	SJ	Granitic clast	See text			1	BFC104

[a] YS = Yellowstone; SJ = San Juan Volcanic Field.
[b] Δ = thermally annealed; CA = chemically abraded.

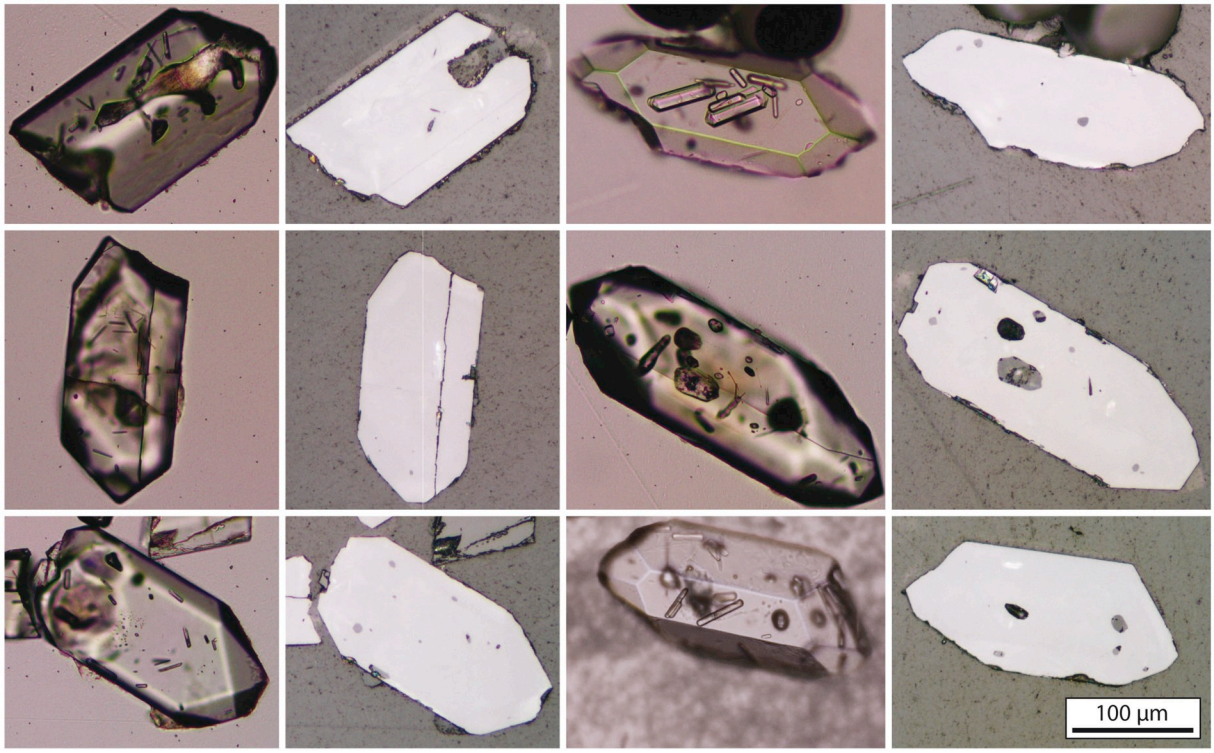

Fig. 1. Comparison of plane polarized light light (columns 1, 3) and corresponding reflected light (columns 2, 4) images of zircons from the Fish Canyon Tuff. Note that although a zircon may appear clean on the surface, there may be Li-bearing mineral/melt/fluid inclusions just beneath the surface.

Trace element substitution in zircon occurs through a variety of mechanisms (Hoskin and Schaltegger, 2003; Bouvier et al., 2012; Tang et al., 2017 and references therein), of which the "xenotime" substitution is responsible for the greatest proportion of REE incorporation by mass fraction. Here, the tetragonal structures of zircon, $ZrSiO_4$, and xenotime, $(Y,REE)PO_4$, form a solid solution to a limited extent (typically 0.1–1.0%), such that:

$$(Y, REE)^{3+} + P^{5+} = Zr^{4+} + Si^{4+}$$

The combined molar abundance of Y and REE (hereafter referred to simply as "REE" due to the similar cation size and geochemical behavior) typically exceeds that of P, indicating that another substitution process may be at work (Hoskin and Schaltegger, 2003 and references therein). Li^+ has the necessary size and valence to charge balance "excess" REE's at an interstitial site, and its incorporation into zircon was noted in experiments where synthetic zircons (grown in a Li-Mo flux) contain Li concentrations proportional to their REE concentrations (Finch et al., 2001; Hanchar et al., 2001). Meanwhile, Bouvier et al. (2012) and Ushikubo et al. (2008) noted that a modified xenotime substitution with interstitial Li^+ maintains charge balance such that the molar concentrations of REE are approximately equal to those of (P + Li). Finally, the addition of H^+ in an interstitial site may also establish charge balance in the form of:

$$(Li, H)^{+} + (Y, REE)^{3+} = (Zr, Hf)^{4+}$$

Indeed, the incorporation of upwards of 1000 µg g^{-1} H_2O (positively correlated with REE) into the balance calculation has been shown to compensate almost entirely for REE excess in experimental and gabbroic zircons (Trail et al. (2011) and De Hoog et al. (2014), respectively) meaning that H^+ and Li^+ may indeed play a similar role in

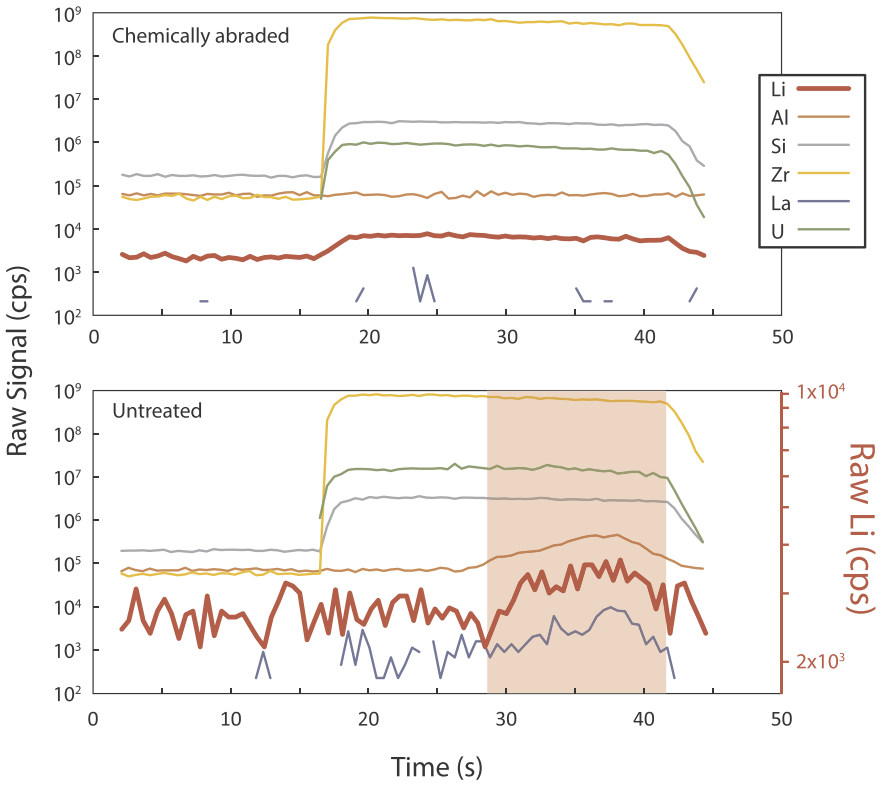

Fig. 2. Comparison of ICP-MS signals from chemically abraded and untreated zircons in counts per s (cps; note enlarged scale at bottom right for Li). While Li concentration is elevated throughout the entire signal in the chemically abraded zircon, the only significant increase in Li in untreated zircons is coincident with increases in Al and La concentrations, indicative of melt and apatite inclusions (respectively).

the zircon crystal lattice. It should be noted that the precise nature of H incorporation (whether by H^+ alone, or as an OH^- complex) is beyond the scope of the present study and is addressed in detail elsewhere (Trail et al., 2011; De Hoog et al., 2014).

On the routine zircon analysis done in our laboratory at ETH Zürich, we regularly observe elevated Li-concentrations (1–100 μg g^{-1}) in chemically abraded and thermally annealed zircons, whereas those that were not treated in this way rarely contain Li above limits of detection (LOD at 3σ confidence is typically < 0.55 μg g^{-1}; calculated after Longerich et al. (1996)). Given the short duration of the annealing procedure, this suggests faster Li diffusion rates in zircon than experimentally determined (Cherniak and Watson, 2010) and consequently, a different diffusion mechanism. The purpose of this study is to demonstrate through natural zircons and experimental procedures that Li mobility in zircon is highly susceptible to low-pressure, high-temperature conditions that are characteristic of thermal annealing, and to suggest a potential mechanism for the seemingly rapid migration of Li. These results are then interpreted in the broader context of Li-in-zircon diffusion chronometry, raising the question of whether magmatic Li diffusion profiles can be overprinted by conditions similar to thermal annealing that can happen during eruption and deposition on the Earth's surface.

2. Methods

2.1. Zircon preparation

Zircons were separated from hand sample with standard techniques, including: pulse fragmentation by SELFRAG, heavy liquid separation by methylene iodide (3.3 g cm^{-3}) and, following chemical abrasion/thermal annealing (if applied), mounting in epoxy and polishing to a finish of < 1 μm by diamond suspension. Chemical abrasion was carried out in two steps: (1) thermal annealing at 850 °C for 48 h in quartz crucibles in ambient atmosphere and (2) partial dissolution in HF. Full details of the procedure can be found in Mattinson (2005) and include (in brief): heating in 48% concentrated HF within Parr vessels at 140 °C for 14 h followed by H_2O and acetone washing steps, overnight 6 N HCl treatment at ~70 °C and a final set of H_2O and acetone washing steps.

2.2. Samples and treatments

Zircons were collected from a variety of volcanic and plutonic units in the Southern Rocky Mountain and Yellowstone Volcanic Fields (Table 1). Mesa Falls Tuff (MFT), Fish Canyon Tuff (FCT) and Nelson Mountain Tuff (NMT) zircons, as well as plutonic zircons from the Mount Princeton Batholith (designation 171516-XX, 71416-XX and 17SJ-XX) were split into two groups and were either thermally annealed (850 °C) or untreated prior to analysis. Other zircons from the San Juan Volcanic Field (designation SRM-XX) underwent either no treatment or the full chemical abrasion procedure (i.e., thermal annealing and HF treatment). Finally, a subset of large FCT zircons from a granitoid clast (sample BFC104) were selected for experiments, undergoing either no treatment, or a variety of treatments, including: piston cylinder and externally-heated pressure vessel annealing (6 and 2 kbar, respectively), gas mixing furnace annealing at ambient pressure as well as regular annealing procedures (see "Experimental procedures" below).

2.3. Laser ablation Inductively-coupled-plasma mass spectrometry (LA-ICP-MS)

Data were collected at ETH Zürich using an ASI Resolution 193 nm ArF excimer laser paired with a Laurin Technic 155 constant geometry 2-volume ablation cell and Thermo Element XR sector field ICP-MS. Laser ablation was performed under pure He atmosphere (0.5–0.7 l/min), after which the ablated material was mixed with Ar in the ablation funnel, homogenized in a signal smoothing device and transported to the ICP. For more details, see Appendix S1.

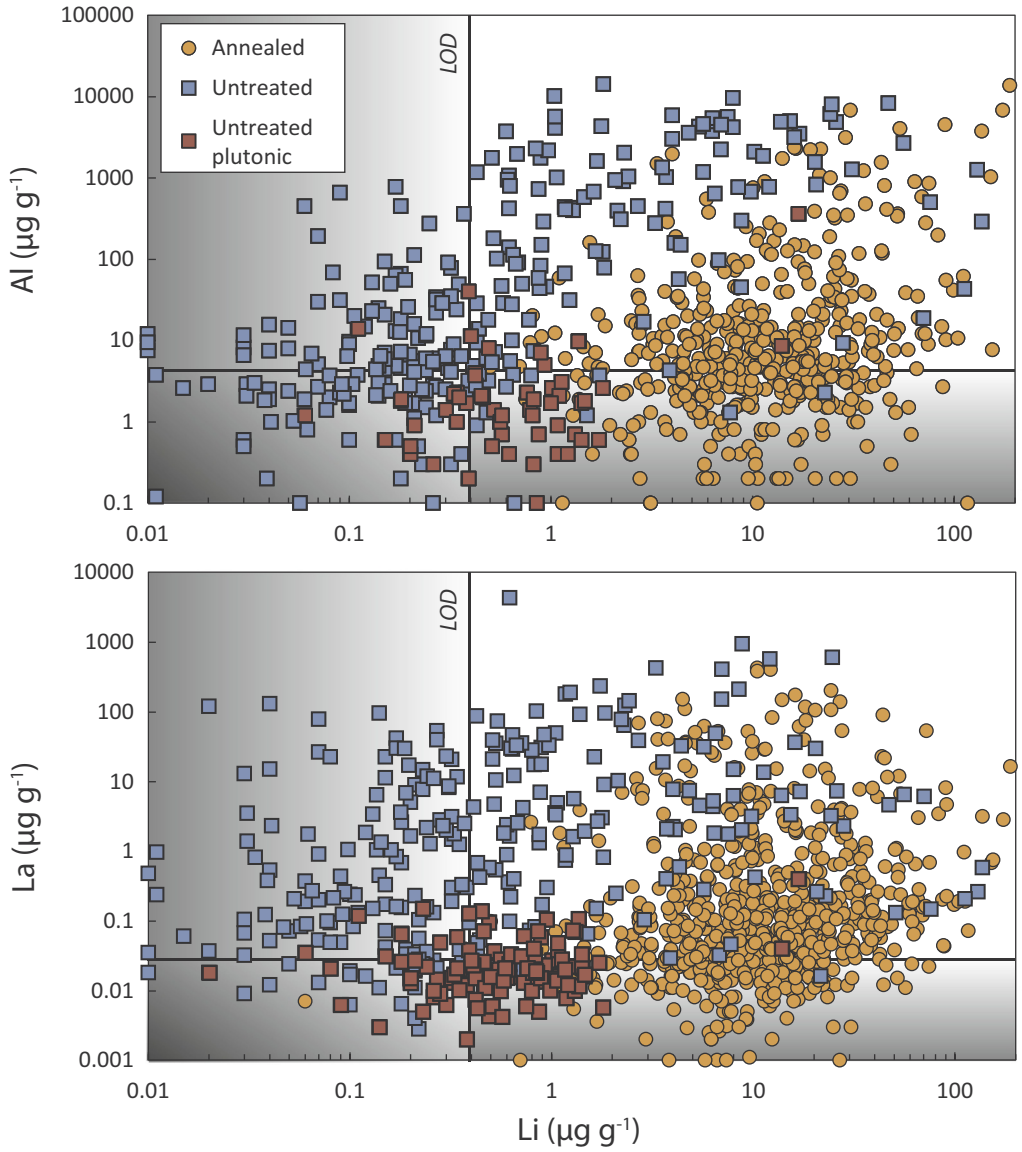

Fig. 3. Li vs Al and La ($\mu g\ g^{-1}$) for annealed (thermally annealed and/or chemically abraded) and untreated zircons prior to data filtering. Values below LOD are plotted in grey boxes. Note that while annealed zircons contain significant concentrations of Li, untreated zircons typically contain Li where Al or La concentrations are high, indicating that a melt or mineral inclusion has been ablated. Also note slightly elevated Li concentrations in plutonic untreated zircons. Error bars excluded for clarity; see other figures for representative uncertainties.

2.4. Experimental procedures

To investigate the factors that influence Li mobility in zircon, several annealing experiments were undertaken using zircons from the Fish Canyon Tuff (sample BFC104), each at 850 °C for 48 h, while a portion of these zircons were untreated and served as a control. In brief:

1) Annealing at ambient pressure and oxygen fugacity (standard procedure; also performed at 700 °C for 24 h)
2) Annealing at ambient pressure and highly reducing conditions (gas mixing furnace)
3) Annealing at 2 kbar in rhyolitic glass at redox conditions corresponding to the Ni-NiO (NNO) oxygen reference buffer (externally-heated pressure vessel; EHPV)
4) Annealing at 6 kbar in rhyolitic glass at redox conditions of the Ni-NiO (NNO) buffered by NNO (piston cylinder).

To rule out the quartz crucible as a source of Li, all experiments were performed in noble metal (Au, Pt or AuPd) crucibles/capsules. However, additional trace element analysis of the quartz crucible routinely used for thermal annealing revealed Li concentrations below detection ($< 0.55\ \mu g\ g^{-1}$, see Appendix S2). For more details about experimental apparatus and run conditions, see Appendix S3.

3. Results

Optical examination of zircons by transmitted light in polished cross-section reveals that inclusion-free zircons are exceptionally rare, and inclusions are often present under the surface and may not be detectable by reflected light (Fig. 1). These inclusions are manifested in LA-ICP-MS analysis as signals of Al (typically $> 20\ \mu g\ g^{-1}$), La ($> 1\ \mu g\ g^{-1}$), and other non-zircon elements (e.g. Na, K, Rb; see Appendix S4), and are nearly always present when Li is detected in untreated zircons (Fig. 2, bottom; Fig. 3).

Chemically abraded and thermally annealed (collectively referred to as "annealed") zircons, on the other hand, display strong and homogeneous Li signals in the absence of inclusions (Fig. 2, top). Here, zircons contain over an order of magnitude higher Li concentration on

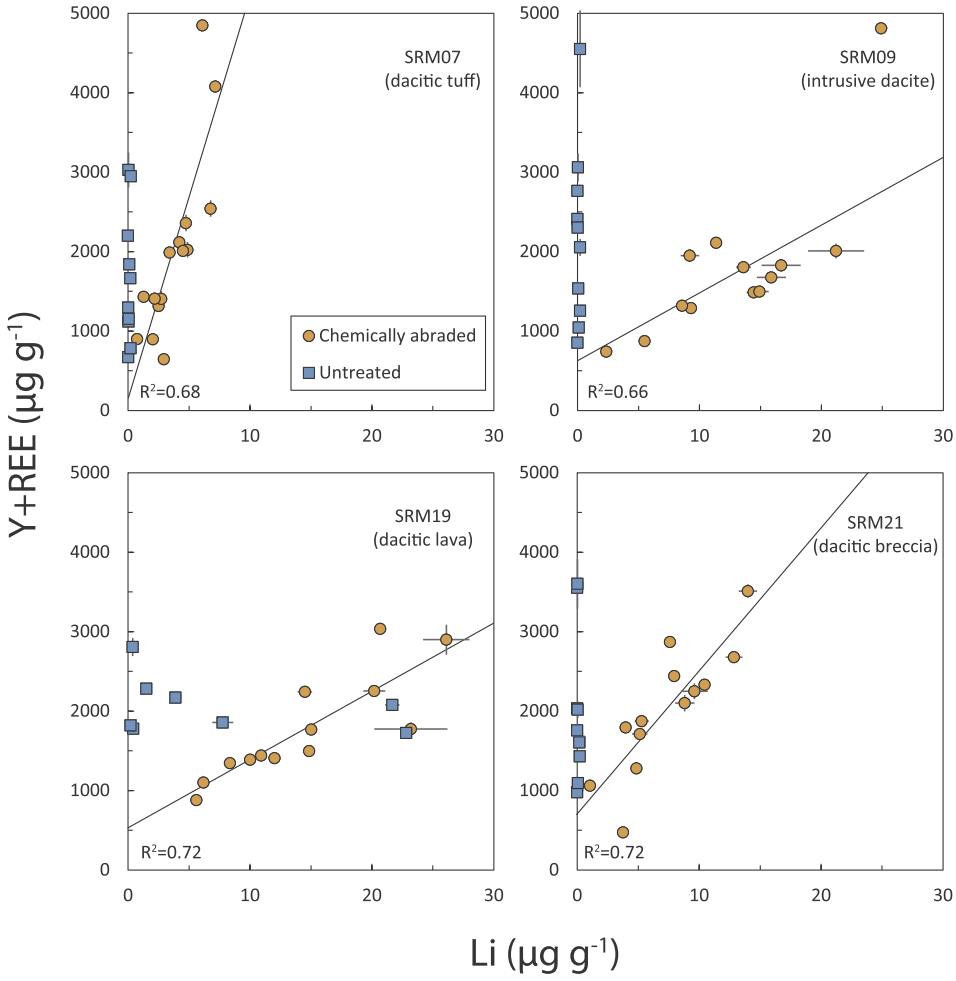

Fig. 4. Y + REE vs Li (µg g^{-1}) for chemically abraded and untreated SRMVF zircons. Note that untreated zircons register no measurable Li concentration, aside from SRM19 (Fisher Dacite lava). All chemically abraded samples contain Li concentrations which are well-correlated with REE concentrations. Values below LOD plotted as 0 and error bars represent 2 SE.

average (4–40 µg g^{-1} vs 0–2 µg g^{-1}), compared to both volcanic and plutonic untreated zircons (Fig. 4). Treatment by chemical abrasion yields an increase in Li concentration in SRMVF zircons (3–30 µg g^{-1}), positively correlated with REE (typically 1000–5000 µg g^{-1}), although one dacitic lava sample shows appreciable Li concentration prior to treatment (Fig. 4, lower left). It should be noted that although strong positive correlations exist ($R^2 > 0.6$), the slopes of the regression lines are quite variable.

Thermal annealing alone produces similar results, as demonstrated by Figs. 5 and 6. Here, zircons from eight samples of the Nelson Mountain Tuff demonstrate a pronounced increase in Li (up to 60 µg g^{-1}) correlated with REE concentration, having registered little or no Li prior to treatment (Fig. 5, bottom right; limit of detection (LOD) ≈ 0.8 µg g^{-1}). Regression lines show similarly high R^2 values (> 0.6), although slopes of regression lines differ between samples. Finally, zircons from plutonic lithologies demonstrate an increase in Li following thermal annealing (up to ~25–40 µg g^{-1}), although a subset of untreated zircons also register a minor amount of Li (< 2 µg g^{-1}; Figs. 6, S4).

3.1. Experimental results

Zircons used for experiments show no detectable traces of Li prior to annealing, and respond to the standard annealing procedure in a similar way to other thermally annealed zircons (i.e. Li concentration of ~1–7 µg g^{-1}; Fig. 7). Annealing in a gas mixing furnace under pure H_2 and ambient pressure (reducing conditions) yields similar results as annealing under standard (oxidizing) conditions, while annealing at lower temperature and for a shorter duration (700 °C for 24 h) under oxidizing conditions generates measurable concentrations of Li which are *poorly* correlated with REE concentration. Meanwhile, annealing in the piston cylinder (850 °C, 48 h; 6 kbar) yields Li concentration below detection within the zircon matrix. Annealing at intermediate pressure in the EHPV (850 °C; 48 h; 2 kbar) yields similarly low concentrations. Slightly elevated Li concentrations in some of these analyses are typically not significant, as they are within error of their individual LOD (Fig. 7, right). Here, Li concentrations in zircons are divided by their individual LOD, and values less than or equal to 1 are considered insignificant.

4. Discussion

4.1. Lithium storage in zircon

Chemical abrasion of zircons was pioneered by Mattinson (2005) for isotope dilution thermal ionization mass spectrometry (ID-TIMS) U-Pb zircon dating and involves both thermal annealing and chemical dissolution steps. While the method or aspects of it are now commonly implemented prior to SIMS (Kryza et al., 2012; Watts et al., 2016) and LA-ICP-MS analyses (Allen and Campbell, 2012; Marillo-Sialer et al., 2016; Sliwinski et al., 2017; Thompson et al., 2018; Ver Hoeve et al., 2018), its effects on Li migration have not yet been addressed.

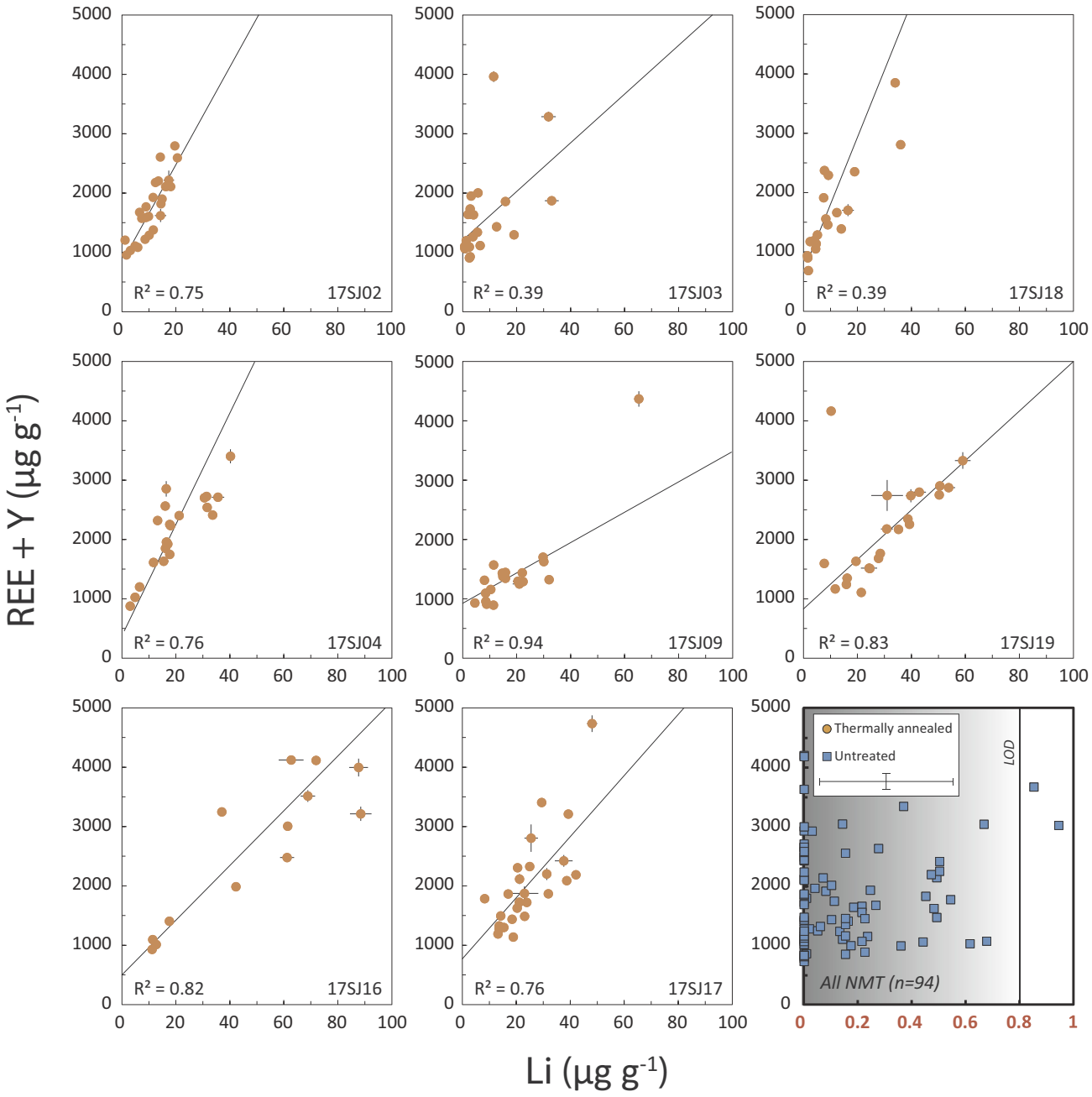

Fig. 5. Li vs REE concentration (µg g^{-1}) for thermally-annealed Nelson Mountain Tuff zircons. Strong correlations exist between these elements for annealed zircons ($R^2 > 0.7$). Outliers are excluded from the regression. Bottom right: untreated zircons demonstrating no detectable Li concentration. Note the change in x axis, and the typical 2 SE uncertainty. Typical LOD for this analytical session was elevated relative to others (typically ~0.4 µg g^{-1}).

Examination of hundreds of signals from multiple analytical sessions in our laboratory at ETH revealed detectable concentrations of Li (typically > 0.4 µg g^{-1}) in the zircon lattice in nearly all analyses, but typically *only* when zircons were thermally annealed or chemically abraded beforehand (Figs. 3–7). The fact that both thermally-annealed zircons and those that had undergone the entire chemical abrasion procedure contained measurable concentrations of Li suggests that Li is most likely introduced into the crystal lattice during the thermal annealing step, and is not related to contamination from chemical reagents. It is also highly unlikely that Li is derived from the quartz annealing crucible, given the low Li concentration in the crucible (< 0.55 µg g^{-1}, see Appendix S2), as well as the high concentration of Li in zircons following annealing in a Au-Pd capsule (Fig. 7).

Studying Li concentrations in untreated zircons reveals that concentrations above the LOD are nearly always correlated with Al, La or other elements atypical for zircon but indicative of mineral or fluid/melt-inclusions (Figs. 2, 3). Indeed, many studies have shown that Li is often sequestered in fluid and melt inclusions (Webster et al., 1996; Wallace et al., 1999; Kobayashi et al., 2004; Teng et al., 2006; Zajacz et al., 2009; Hofstra et al., 2013), making them likely sources for Li introduced into the crystal lattice. Finally, it should also be noted that Li is generally incompatible in zircon. Cherniak and Watson (2010) demonstrated Li-in-zircon concentrations on the order of 100–600 µg g^{-1} in a source containing ~10,000–20,000 µg g^{-1} Li following experimental runs, which equates to a D_{Li} of ~0.005–0.06. This observation is seemingly at odds with many studies that hypothesize a role for Li^+ in charge-balancing REE in zircon, and will be discussed below.

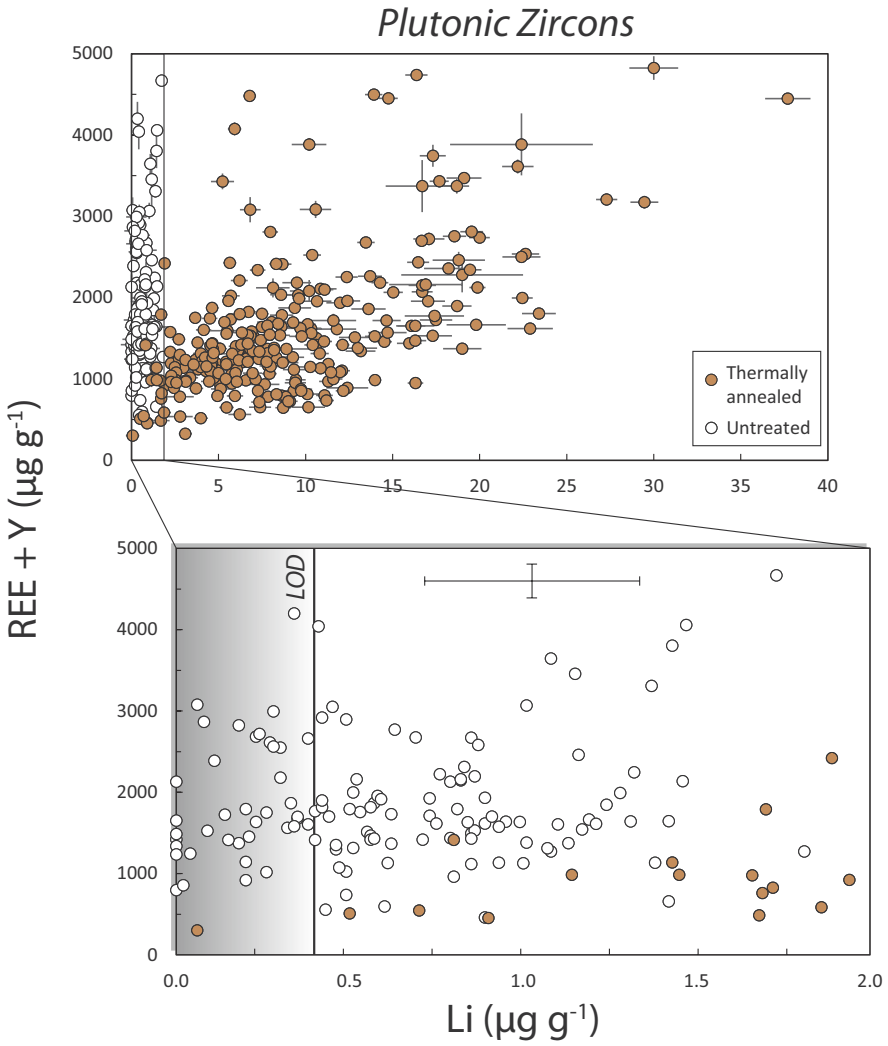

Fig. 6. Li vs REE ($\mu g\, g^{-1}$) trends for untreated (bottom; top inset) and thermally annealed (top) samples from the Mount Princeton Batholith and surrounding ring dykes. Note that thermal annealing increases the Li concentration of zircons in a manner proportional to REE concentrations. Meanwhile, untreated zircons typically have low ($< 2\, \mu g\, g^{-1}$) or < LOD concentrations of Li. Typical 2 SE error bar and LOD ($\sim 0.4\, \mu g\, g^{-1}$) shown.

4.2. Lithium diffusion in zircon

Many zircons demonstrate *homogeneous* Li signals correlated with REE concentrations after annealing (Figs. 3–7), which enables the estimation of Li diffusion rates using the "center retention" criteria of Cherniak and Watson (2010). Here, an estimate is provided for the maximum time that a hypothetical spherical zircon can retain a distinguishable chemical domain at its center, assuming that the melt/fluid inclusion is the "chemical domain" that is being homogenized by diffusion. Due to the strong correlation between REE and Li, it is safe to assume that the Li concentration has permeated throughout the lattice and reached equilibrium with the chemical environment of the zircon (i.e., the maximum time of "center retention" has been exceeded). Zircons in this study typically have radii of < 50 µm, defining the upper limit of the Li diffusion distance, and due to the typical spacing between inclusions, one can assume Li has diffused at least ~10 µm (Fig. 8). Using these parameters and applying the model of Cherniak and Watson (2010):

$$D_{Li} = 7.17{*}10^{-7} \exp(-275 \pm 11\ \text{kJ mol}^{-1})/RT)\ \text{m}^2\ \text{s}^{-1}$$

It is possible to obtain a diffusion coefficient at 850 °C; combined with the diffusional radii obtained above, this results in maximum retention times of ~300–7000 days for 10–50 µm of diffusional radii (Fig. 9). This is roughly 2–3 orders of magnitude *longer* than the time frame of 48 h employed in this study and typically employed to anneal zircons for analysis.

This apparent discrepancy between diffusion rates in the present study and those of Cherniak and Watson (2010) and Trail et al. (2016) suggests that there are different modes of Li diffusion operating in zircon. This disagreement was already alluded to in previous studies. For example, Ushikubo et al. (2008) and Tang et al. (2017) took note of *prolonged* retention of Li in zircon, with the latter proposing multi-mode diffusion involving "slow" (coupled REE with Li) and "fast" (uncoupled REE and Li) diffusion processes. "Slow" diffusion was invoked to explain unexpectedly sharp Li gradients in the presence of prolonged thermal histories of igneous and granulite-facies zircons. According to these two studies, the experimentally-determined diffusion coefficients are *too fast*, which in part led Wilson et al. (2017) to question the assertions of Rubin et al. (2017) that their magmatic zircons had experienced a limited (< 100 yr) history at super-solidus conditions. Cooper et al. (2017) asserted that there was no direct evidence provided by Tang et al. (2017) or Wilson et al. (2017) for multi-mode diffusion in the form of REE vs Li correlations, nor is there at present any way to determine the conditions under which the "slow" (REE-controlled) charge-coupled diffusion mechanism would become dominant. In response to authors on both sides of the debate, it is proposed that:

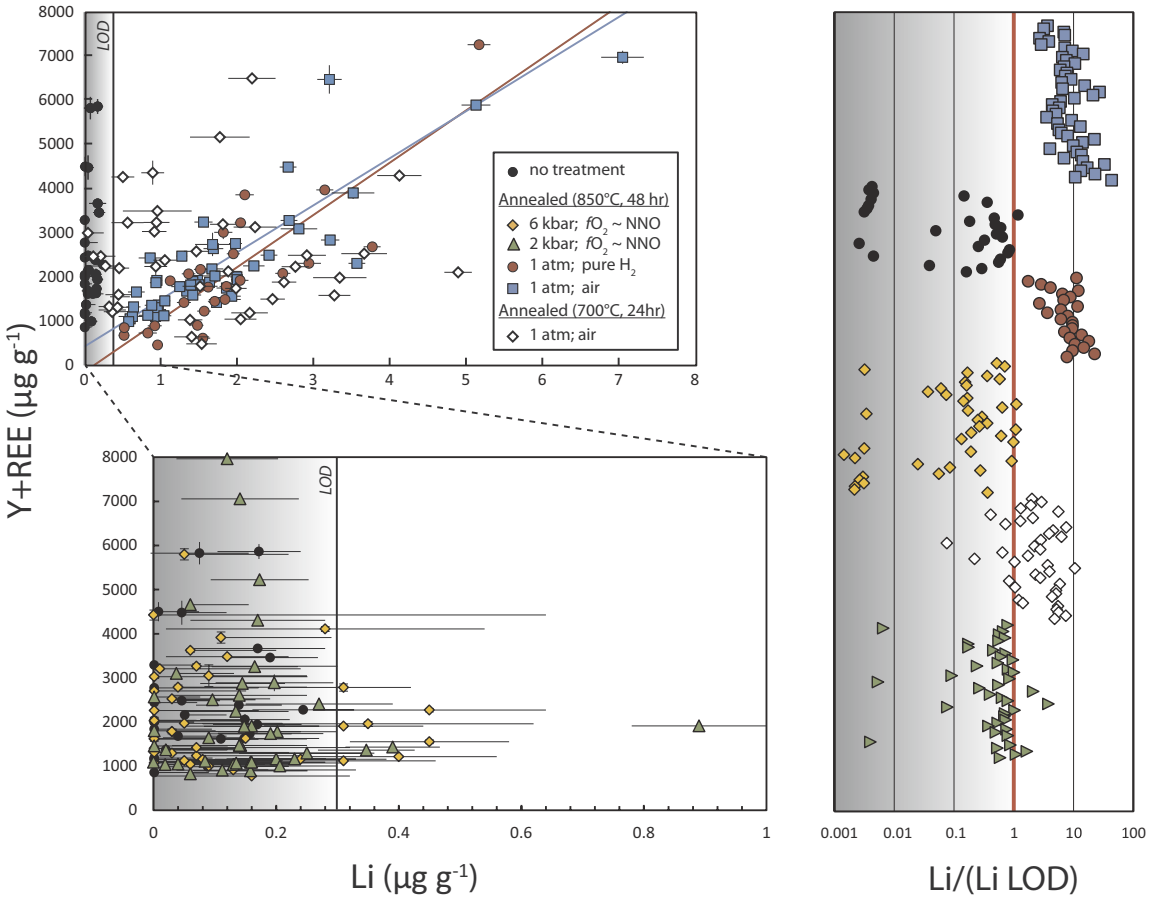

Fig. 7. Li vs REE trends for experimentally-treated zircons (sample BFC104): Untreated zircons (black circles) contain Li below the limit of detection (typically 0.3–0.4 µg g^{-1}), while zircons annealed under oxidizing conditions at 850 °C (blue squares; air) contain measurable Li positively correlated with REE concentrations (blue regression line). A similar experiment under reducing conditions (red squares) results in a similar trend (red regression line). Annealing under oxidizing conditions at 700 °C for a shorter duration of 24 h also results in measurable Li concentrations, though poorly correlated with REE concentration (white diamonds). Meanwhile, annealing at 850 °C for 48 h at 6 or 2 kbar pressure (yellow diamonds and green triangles, respectively) results in Li concentrations below the detection limit. Because the LOD is somewhat sample-dependent, analyses are plotted on the right against their individual LOD's. (For interpretation of the references to color in this figure legend, the reader is referred to the web version of this article.)

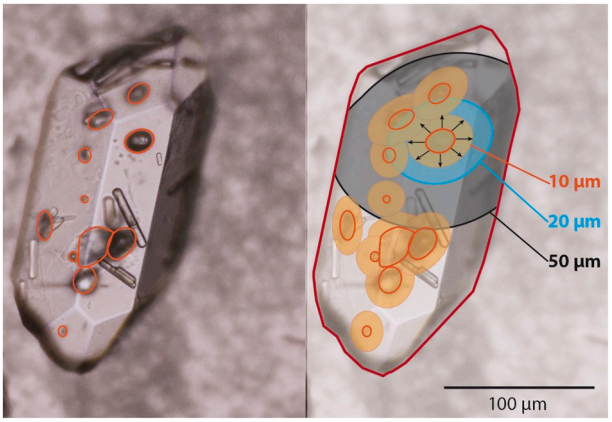

Fig. 8. Left: plane polarized light light photomicrograph of a typical zircon from the Fish Canyon Tuff, with melt/fluid inclusions outlined in orange. Right: Diffusional distances of 10, 20 and 50 µm from the selected inclusions outlined, demonstrating that Li must diffuse between 10 and 50 µm from inclusions in order to permeate the zircon lattice.

1. Li does indeed diffuse toward and couple with REE following thermal annealing. This is not due to the diffusion of the latter, as these trivalent cations diffuse orders of magnitude slower than Li (Cherniak, 2010) and cathodoluminescence patterns in zircons show no sign of homogenization after annealing. Rather, it is Li that moves and accumulates in concentrations proportional to the pre-existing REE contents.
2. The discrepancy in diffusion rates among various authors may be explained by the fundamental differences between the diffusion experiments of Cherniak and Watson (2010) and natural, inclusion-rich zircons (detailed below).

The first point follows the observation that post-annealing zircon trace element data demonstrates a clear and strong correlation between REE and Li (Figs. 3–7), and is consistent with trends observed in synthetic zircon experiments (Finch et al., 2001) and in natural zircons (Ushikubo et al., 2008; Grimes et al., 2011; Bouvier et al., 2012; De Hoog et al., 2014; Gao et al., 2015; Trail et al., 2016; Tang et al., 2017). The lack of these trends observed by Rubin et al. (2017) may indicate that Li is out of equilibrium with respect to its chemical environment (therefore suitable for diffusion speedometry), but it is likely that these zircons cannot be treated in the same context as the experiments performed by Cherniak and Watson (2010).

Diffusion rate experiments performed by Cherniak and Watson (2010) consisted of Mud Tank zircons pre-annealed at 1300 °C prior to being placed in a Li-Zr-REE starting material and subjected to variable pressure, temperature and water activity (Fig. 10a, b). Because of the high–temperature annealing step, it is safe to assume that the zircons

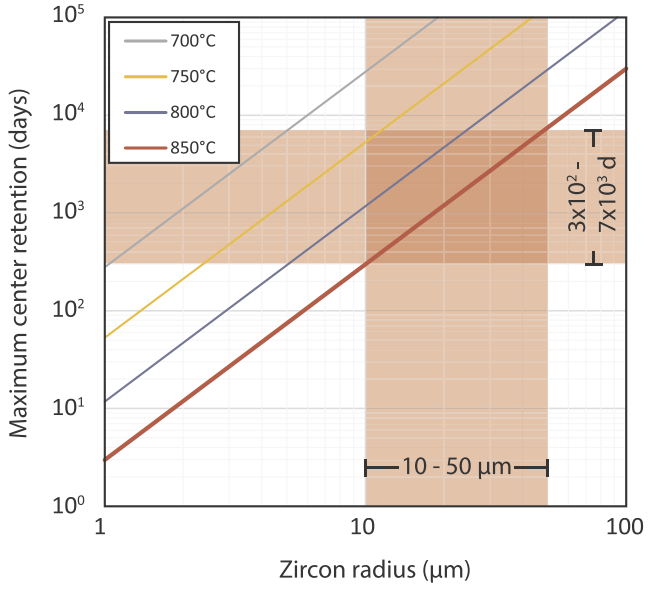

Fig. 9. Center-retention time for zircons of variable radii at variable temperatures. Note that retention times for 10–50 μm diffusion radii at 850 °C are ~300–7000 days, but that the center retention criterion has been exceeded in thermally-annealed zircons in 48 h, or approximately ~100–1000 times faster than experimental diffusion coefficients suggest.

were at chemical equilibrium (with respect to Li and H) prior to the start of the experiments. Varying the Li concentration and the water activity of the experimental medium had no effect on the diffusion rate of Li in these experiments, which obeys the classical notion that it is the chemical *potential*, not the gradient, which determines the diffusion rate (Zhang, 2010). In other words, while there may have been variable steep Li and H *gradients* pushing diffusion in these experiments, the chemical *potentials* of both were essentially equivalent in all experiments as the zircons were already at equilibrium with regard to Li and H.

By contrast, inclusion-rich zircons in actively erupting regimes (Fig. 10c) exist under extreme disequilibrium characterized by a strong volatile chemical potential gradient (H_2O, Li, etc.) between inclusions and the environment, which is not present in deeper magma reservoirs (or in constant pressure, constant f_{H2O} diffusion experiments). If one assumes that melt inclusions in zircons were entrapped under water-rich to water-saturated conditions (Fig. 10d) and considers that H_2O solubility in rhyolitic melts decreases drastically at ambient pressure (Holtz et al., 2001), it follows that melt inclusions at ambient pressures and elevated temperatures (i.e. in syn-eruptive conditions, Fig. 10c) are strongly H_2O-oversaturated and must impart pressure on the crystal lattice if they are heated above their solidi (which is also true for Li, though the lower volatility and much lower concentration of Li diminish this effect). This deduction, combined with the likely role of H^+ in the zircon lattice (De Hoog et al., 2014), the source of Li in zircons and the rapid gain of Li after annealing, leads us to propose a theoretical model for Li diffusion under eruptive/annealing conditions:

H^+ is the primary charge-balancing agent for excess REE^{3+} in zircon and occupies interstitial sites in the crystal lattice, while Li is

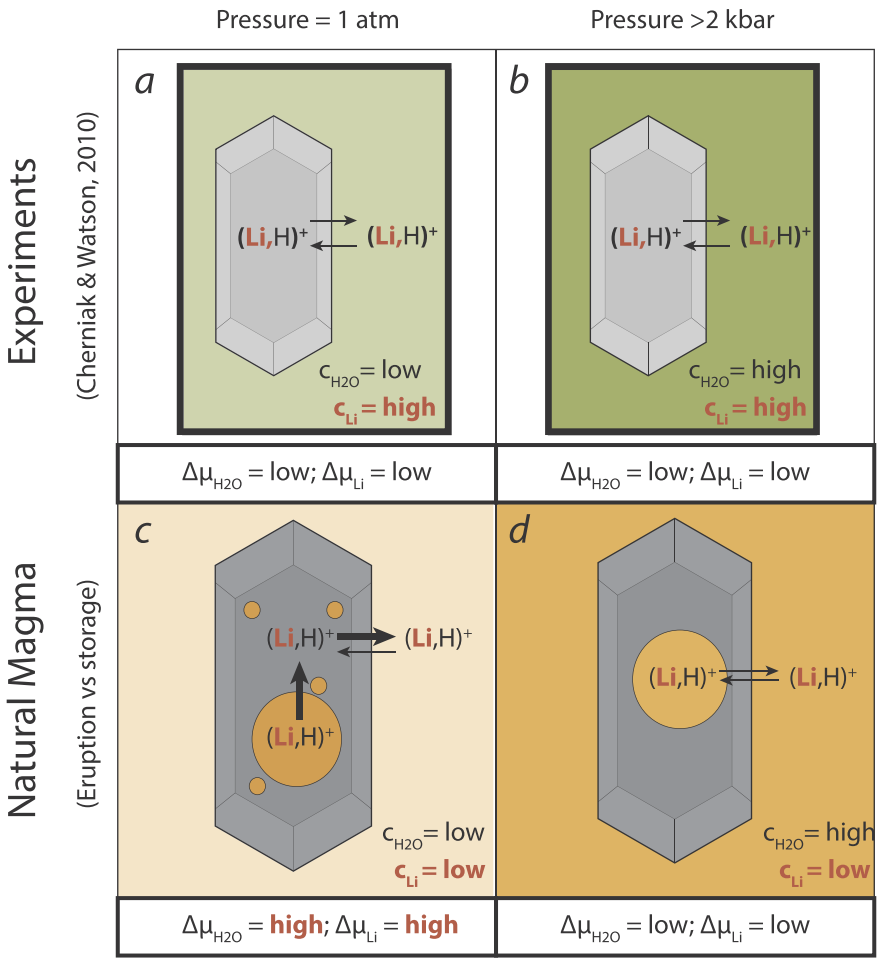

Fig. 10. Schematic for Li^+ and H^+ mobility under variable experimental and natural conditions. (a, b) Experiments performed by Cherniak and Watson (2010) utilize the Mud Tank zircon. Due to prior annealing, this zircon is at chemical equilibrium during the in-diffusion experiments and therefore shows similar rates of Li diffusion under dry (a) and wet (b) conditions as the chemical potential ($\Delta\mu_{H2O}$) is low in both cases. (c, d) Zircons crystallizing under water-saturated conditions entrap melt inclusions (d) with similar Li and H_2O concentrations, and are at equilibrium with the host melt ($\Delta\mu_{H2O}$ is low). Large REE concentrations are in excess of what can be charge balanced by P^{5+}, and H^+ presumably provides the addition charge balance. Under eruptive conditions (c), the zircon matrix loses H^+ to the volatile phase, generating a strong $\Delta\mu_{H2O}$ and providing an additional driving force for Li^+ diffusion.

incompatible and is retained in melt/fluid inclusions. A net loss of H^+ to the environment can occur if there is a strong H^+ potential from within, and if resulting charge vacancies are occupied by monovalent cations. Heating of zircons to supersolidus temperatures (with respect to melt inclusions) at ambient pressures results in the exsolution of volatiles from melt inclusions and triggers a net loss of H^+ from the zircon. Under such conditions, both H^+ and Li^+ are expelled from melt/fluid inclusions and occupy vacancies in the crystal lattice proportional to the pre-existing $(Y + REE)^{3+}$ concentration at rates much faster than previously determined.

4.3. Li diffusion in experimental and natural samples

This model of Li migration as a secondary feature of H^+ loss is supported experimentally under various conditions. While regular annealing procedures lead to pronounced Li gain by the zircon lattice, annealing at the same temperature and duration at *elevated pressure and fluid (H_2O)-saturated conditions* (6 kbar, likely much greater than the pressure of melt inclusion entrapment) inhibits Li mobility almost entirely, as does annealing at intermediate pressure (2 kbar; Fig. 7). To exclude the possibility that redox disequilibrium is responsible for Li migration, an experiment was performed in a gas mixing furnace under pure H_2 (reducing) atmosphere, with nearly identical results to the regular annealing procedure under oxidizing (atmospheric) conditions. Finally, because 850 °C is unrealistically high for some water-saturated rhyolites, an experiment was performed in a standard annealing oven at 700 °C for 24 h, with results pointing to significant Li migration characterized by its elevated concentration, albeit poorly-correlated with REE (Fig. 7). Collectively, these experiments demonstrate that Li mobility (and hence, diffusional profiles) are heavily susceptible to syn-eruptive near-isothermal depressurization at much faster timescales than experimentally determined (2 days vs 300–7000 days), and should therefore be treated with extreme caution before being used to infer magmatic time-temperature conditions.

The proposed model is also consistent with the predicted behavior of Li in zircons from the diverse array of magmatic products in this study. Plutonic zircons (Fig. 6; SRM09 of Fig. 4) seldom have measurable Li, which is consistent with the incompatibility of Li in zircon and holding of these systems at high pressures during cooling from sub- to solidus conditions. The occasional measurable Li concentration in these zircons may be a result of the prolonged cooling of the magma (allowing for minor diffusion) during progressive degassing of the reservoir, which allows for reequilibration of melt inclusion Li and H contents with the host silicate melt. Zircons from the ***lava flow*** sample (SRM19) contain measurable Li prior to annealing, consistent with prolonged cooling at ambient pressures that lavas typically experience. Most other zircon samples are from ignimbrites, which, having been rapidly quenched during eruption, seldom contain measurable Li until thermally annealed. It should be noted that while these samples were "quenched" to the point that the Li content of the melt inclusions did not *completely* permeate the zircon lattice, it is unclear whether *any* inclusion-driven Li migration occurred in these samples. The concentration- and length-scales studied by NanoSIMS (Rubin et al., 2017) are not resolvable by LA-ICP-MS ($ng\,g^{-1}$ vs $\mu g\,g^{-1}$ detection limits and 30 μm vs 1 μm spatial resolution, respectively), therefore minor perturbations of Li diffusional patterns by rapid isothermal depressurization within the volcanic conduit cannot be observed. However, such low-concentration and short-range diffusional profiles would be consistent with a system that had experienced several hours of reduced pressure above the solidus of the melt inclusions (either due to upward magma migration in the conduit, or reheating in a pyroclastic density current).

5. Conclusions

By studying natural zircons both before and after annealing, it is demonstrated that Li may diffuse through the zircon lattice at rates much faster than conventional Li diffusion experiments predict. It is proposed that Li diffusion during thermal annealing/chemical abrasion at elevated temperatures and ambient pressures (mimicking eruptive conditions) follows a mechanism different than that invoked by Cherniak and Watson (2010), with H_2O-oversaturated melt inclusions providing a strong chemical potential gradient that leads to indiscriminate and rapid Li^+ and H^+ permeation of the crystal lattice. In particular, it is proposed that H^+ plays an important role in charge-balancing trivalent $(Y,REE)^{3+}$ cations under magmatic conditions (De Hoog et al., 2014), and its incorporation into the zircon lattice provides a conduit for reequilibration of H_2O between melt inclusions and the surrounding environment during eruptive conditions. In this model, the chemical potential provided by H_2O is the motive force that allows the Li^+ to occupy the lattice in concentrations proportional to REE.

Given that this process may take place anytime a magma/lava is depressurized (and at a temperature where melt inclusions are above their solidi; i.e. during magma emplacement, within the volcanic conduit, or within lava flows and pyroclastic density currents), this places severe limits on the applicability of Li-in-zircon diffusion speedometry in volcanic samples. In light of recent interest in magmatic Li-in-zircon diffusion speedometry (Rubin et al., 2017), it is important to consider the extreme mobility of Li and H that may result from degassing/eruption of a magma body and overprint pre-existing diffusion profiles.

Supplementary data to this article can be found online at https://doi.org/10.1016/j.chemgeo.2018.09.038.

Acknowledgements

This study was supported by ETH Research Grants ETH-34 15-2 (JS), ETH-14 16-1 (FM) and by Swiss National Science Foundation research grant 200020-153112/1 (NK). We would like to thank Jörn Wotzlaw for providing FCT zircons and Juliana Troch for providing LCT rhyolitic glass. Samples from the SRMVF were collected in part by Matt Zimmerer, Peter Lipman, Chad Deering and Olivia Barbee. In addition, we thank Ben Ellis, Kari Cooper and Christy Till for their input in earlier versions of this manuscript.

References

Allen, C.M., Campbell, I.H., 2012. Identification and elimination of a matrix-induced systematic error in LA-ICP-MS Pb-206/U-238 dating of zircon. Chem. Geol. 332, 157–165. https://doi.org/10.1016/j.chemgeo.2012.09.038.

Bouvier, A.-S., Ushikubo, T., Kita, N.T., Cavosie, A.J., Kozdon, R., Valley, J.W., 2012. Li isotopes and trace elements as a petrogenetic tracer in zircon: insights from Archean TTGs and sanukitoids. Contrib. Mineral. Petrol. 163 (5), 745–768.

Cherniak, D.J., 2010. Diffusion in accessory minerals: zircon, titanite, apatite, monazite and xenotime. Rev. Mineral. Geochem. 72 (1), 827–869.

Cherniak, D., Watson, E., 2010. Li diffusion in zircon. Contrib. Mineral. Petrol. 160 (3), 383–390.

Coogan, L.A., Kasemann, S.A., Chakraborty, S., 2005. Rates of hydrothermal cooling of new oceanic upper crust derived from lithium-geospeedometry. Earth Planet. Sci. Lett. 240 (2), 415–424.

Cooper, K.M., Till, C.B., Kent, A.J., Costa, F., Rubin, A.E., Gravley, D., Deering, C., Cole, J., Bose, M., 2017. Response to Comment on "Rapid cooling and cold storage in a silicic magma reservoir recorded in individual crystals". Science 358 (6370), eaap9145.

De Hoog, J., Lissenberg, C.J., Brooker, R., Hinton, R., Trail, D., Hellebrand, E., 2014. Hydrogen incorporation and charge balance in natural zircon. Geochim. Cosmochim. Acta 141, 472–486.

Dohmen, R., Kasemann, S.A., Coogan, L., Chakraborty, S., 2010. Diffusion of Li in olivine. Part I: experimental observations and a multi species diffusion model. Geochim. Cosmochim. Acta 74 (1), 274–292.

Ellis, B.S., Cordonnier, B., Rowe, M.C., Szymanowski, D., Bachmann, O., Andrews, G.D., 2015. Groundmass crystallisation and cooling rates of lava-like ignimbrites: the Grey's Landing ignimbrite, southern Idaho, USA. Bull. Volcanol. 77 (10), 87.

Ellis, B., Szymanowski, D., Magna, T., Neukampf, J., Dohmen, R., Bachmann, O., Ulmer, P., Guillong, M., 2018. Post-eruptive mobility of lithium in volcanic rocks. Nat. Commun. 9.

Ferry, J., Watson, E., 2007. New thermodynamic models and revised calibrations for the Ti-in-zircon and Zr-in-rutile thermometers. Contrib. Mineral. Petrol. 154 (4), 429–437. https://doi.org/10.1007/s00410-007-0201-0.

Finch, R.J., Hanchar, J.M., Hoskin, P.W., Burns, P.C., 2001. Rare-earth elements in synthetic zircon: part 2. A single-crystal X-ray study of xenotime substitution. Am. Mineral. 86 (5–6), 681–689.

Gao, Y.-Y., Li, X.-H., Griffin, W.L., Tang, Y.-J., Pearson, N.J., Liu, Y., Chu, M.-F., Li, Q.-L., Tang, G.-Q., O'Reilly, S.Y., 2015. Extreme lithium isotopic fractionation in three zircon standards (Plešovice, Qinghu and Temora). Sci. Rep. UK 5.

Giletti, B.J., Shanahan, T.M., 1997. Alkali diffusion in plagioclase feldspar. Chem. Geol. 139 (1–4), 3–20.

Grimes, C.B., Ushikubo, T., John, B.E., Valley, J.W., 2011. Uniformly mantle-like δ18O in zircons from oceanic plagiogranites and gabbros. Contrib. Mineral. Petrol. 161 (1), 13–33.

Hanchar, J.M., Finch, R.J., Hoskin, P.W., Watson, E.B., Cherniak, D.J., Mariano, A.N., 2001. Rare earth elements in synthetic zircon: part 1. Synthesis, and rare earth element and phosphorus doping. Am. Mineral. 86 (5–6), 667–680.

Hofstra, A.H., Todorov, T., Mercer, C., Adams, D., Marsh, E., 2013. Silicate melt inclusion evidence for extreme pre-eruptive enrichment and post-eruptive depletion of lithium in silicic volcanic rocks of the Western United States: implications for the origin of lithium-rich brines. Econ. Geol. 108 (7), 1691–1701.

Holtz, F., Johannes, W., Tamic, N., Behrens, H., 2001. Maximum and minimum water contents of granitic melts generated in the crust: a reevaluation and implications. Lithos 56 (1), 1–14.

Hoskin, P.W., Schaltegger, U., 2003. The composition of zircon and igneous and metamorphic petrogenesis. Rev. Mineral. Geochem. 53 (1), 27–62.

Kobayashi, K., Tanaka, R., Moriguti, T., Shimizu, K., Nakamura, E., 2004. Lithium, boron, and lead isotope systematics of glass inclusions in olivines from Hawaiian lavas: evidence for recycled components in the Hawaiian plume. Chem. Geol. 212 (1), 143–161.

Kryza, R., Crowley, Q.G., Larionov, A., Pin, C., Oberc-Dziedzic, T., Mochnacka, K., 2012. Chemical abrasion applied to SHRIMP zircon geochronology: an example from the Variscan Karkonosze Granite (Sudetes, SW Poland). Gondwana Res. 21 (4), 757–767. https://doi.org/10.1016/j.gr.2011.07.007.

Li, X.-H., Li, Q.-L., Liu, Y., Tang, G.-Q., 2011. Further characterization of M257 zircon standard: a working reference for SIMS analysis of Li isotopes. J. Anal. At. Spectrom. 26 (2), 352–358.

Longerich, H.P., Jackson, S.E., Günther, D., 1996. Inter-laboratory note. Laser ablation inductively coupled plasma mass spectrometric transient signal data acquisition and analyte concentration calculation. J. Anal. Atom. Spectrom. 11 (9), 899–904.

Magna, T., Wiechert, U., Halliday, A.N., 2006. New constraints on the lithium isotope compositions of the Moon and terrestrial planets. Earth Planet. Sci. Lett. 243 (3), 336–353.

Marillo-Sialer, E., Woodhead, J., Hanchar, J.M., Reddy, S.M., Greig, A., Hergt, J., Kohn, B., 2016. An investigation of the laser-induced zircon 'matrix effect'. Chem. Geol. 438, 11–24. https://doi.org/10.1016/j.chemgeo.2016:05.014.

Mattinson, J.M., 2005. Zircon U-Pb chemical abrasion ("CA-TIMS") method: combined annealing and multi-step partial dissolution analysis for improved precision and accuracy of zircon ages. Chem. Geol. 220 (1–2), 47–66. https://doi.org/10.1016/j.chemgeo.2005.03.011.

Rubin, A.E., Cooper, K.M., Till, C.B., Kent, A.J., Costa, F., Bose, M., Gravley, D., Deering, C., Cole, J., 2017. Rapid cooling and cold storage in a silicic magma reservoir recorded in individual crystals. Science 356 (6343), 1154–1156.

Rudnick, R.L., Tomascak, P.B., Njo, H.B., Gardner, L.R., 2004. Extreme lithium isotopic fractionation during continental weathering revealed in saprolites from South Carolina. Chem. Geol. 212 (1), 45–57.

Sliwinski, J.T., Guillong, M., Liebske, C., Dunkl, I., Von Quadt, A., Bachmann, O., 2017. Improved accuracy of LA-ICP-MS U-Pb ages of Cenozoic zircons by alpha dose correction. Chem. Geol. 472, 8–21.

Tang, M., Rudnick, R.L., McDonough, W.F., Bose, M., Goreva, Y., 2017. Multi-mode Li diffusion in natural zircons: evidence for diffusion in the presence of step-function concentration boundaries. Earth Planet. Sci. Lett. 474, 110–119.

Teng, F.-Z., McDonough, W.F., Rudnick, R.L., Walker, R.J., Sirbescu, M.-L.C., 2006. Lithium isotopic systematics of granites and pegmatites from the Black Hills, South Dakota. Am. Mineral. 91 (10), 1488–1498.

Thompson, J.M., Meffre, S., Danyushevsky, L., 2018. Impact of air, laser pulse width and fluence on U–Pb dating of zircons by LA-ICPMS. J. Anal. At. Spectrom. 33 (2), 221–230.

Trail, D., Thomas, J.B., Watson, E.B., 2011. The incorporation of hydroxyl into zircon. Am. Mineral. 96 (1), 60–67.

Trail, D., Cherniak, D.J., Watson, E.B., Harrison, T.M., Weiss, B.P., Szumila, I., 2016. Li zoning in zircon as a potential geospeedometer and peak temperature indicator. Contrib. Mineral. Petrol. 171 (3), 25.

Ushikubo, T., Kita, N.T., Cavosie, A.J., Wilde, S.A., Rudnick, R.L., Valley, J.W., 2008. Lithium in Jack Hills zircons: evidence for extensive weathering of Earth's earliest crust. Earth Planet. Sci. Lett. 272 (3), 666–676.

Ver Hoeve, T.J., Scoates, J.S., Wall, C.J., Weis, D., Amini, M., 2018. Evaluating downhole fractionation corrections in LA-ICP-MS U-Pb zircon geochronology. Chem. Geol. 483, 201–217.

Wallace, P.J., Anderson, A.T., Davis, A.M., 1999. Gradients in H2O, CO2, and exsolved gas in a large-volume silicic magma system: interpreting the record preserved in melt inclusions from the Bishop Tuff. J. Geophys. Res. Solid Earth 104 (B9), 20097–20122.

Watts, K.E., Coble, M.A., Vazquez, J.A., Henry, C.D., Colgan, J.P., John, D.A., 2016. Chemical abrasion-SIMS (CA-SIMS) U-Pb dating of zircon from the late Eocene Caetano caldera, Nevada. Chem. Geol. 439, 139–151. https://doi.org/10.1016/j.chemgeo.2016.06.013.

Webster, J.D., Burt, D.M., Aguillon, R., 1996. Volatile and lithophile trace-element geochemistry of Mexican tin rhyolite magmas deduced from melt inclusions. Geochim. Cosmochim. Acta 60 (17), 3267–3283.

Wilson, C.J., Morgan, D.J., Charlier, B.L., Barker, S.J., 2017. Comment on "Rapid cooling and cold storage in a silicic magma reservoir recorded in individual crystals". Science 358 (6370), eaap8429.

Zajacz, Z., Hanley, J.J., Heinrich, C.A., Halter, W.E., Guillong, M., 2009. Diffusive re-equilibration of quartz-hosted silicate melt and fluid inclusions: are all metal concentrations unmodified? Geochim. Cosmochim. Acta 73 (10), 3013–3027.

Zhang, Y., 2010. Diffusion in minerals and melts: theoretical background. Rev. Mineral. Geochem. 72 (1), 5–59.